This is the accepted manuscript made available via CHORUS. The article has been published as:

Laboratory experiments modeling the transport and deposition of sediments by glacial plumes rising under an ice shelf

Bruce R. Sutherland, Madelaine G. Rosevear, and Claudia Cenedese

Phys. Rev. Fluids **5**, 013802 — Published 21 January 2020

DOI: 10.1103/PhysRevFluids.5.013802

Laboratory Experiments Modelling the Transport and Deposition of Sediments by Glacial Plumes Rising Under an Ice Shelf

Bruce R. Sutherland,[1,2,*] Madelaine G. Rosevear,[3] and Claudia Cenedese[4]

[1] *Department of Physics, University of Alberta, Edmonton, AB, T6G 2E1, Canada*

[2] *Department of Earth & Atmospheric Sciences, University of Alberta, Edmonton, AB, T6G 2E3, Canada*

[3] *Institute of Marine and Antarctic Studies, University of Tasmania, South Hobart, Australia*

[4] *Woods Hole Oceanographic Institution, Woods Hole, MA, USA*

Abstract

Motivated by the observation of sediments being carried by meltwater plumes originating at the base of a marine terminating glacier, laboratory experiments are performed to examine the transport and deposition of particles settling out from a buoyant line-plume rising along a sloping upper boundary. If the plume source has relatively high momentum and is located near the bottom of the domain, a strong recirculating region develops near the source. Emanating from this region is a particle bearing buoyant plume that moves at near constant speed along the slope. Particles are observed to settle within the plume itself and then descend from the plume toward the tank bottom being drawn back in the direction of the source through a return flow driven by the plume's entrainment of the underlying ambient fluid. A light attenuation technique is employed to measure non-intrusively the depth of the sediment bed after the source is turned off and all the particles settled out. Sediments are found to accumulate near the source over the extent of the recirculating region and then decrease approximately linearly with distance from the source. Conceptual theoretical models suggest that the linearly sloping bed results from a combination of vertical mixing in the plume near the recirculation region and the return flow acting to detrain from the plume particles more effectively near the plume source where the shear between the plume and the return flow is largest. In many aspects the experiments are not representative of a steady glacial meltwater plume due to restrictions of the experimental setup, notably the relatively low Reynolds number of the flow. Nonetheless the experiments are suggestive of the complicated dynamics and sediment deposition patterns that may occur near the base of a marine terminating glacier, with a crude estimate of mean clay deposition at a rate of 6 cm per year over a distance of 2 km from the source.

* Email: bruce.sutherland@ualberta.ca; Web: https://www.ualberta.ca/~bsuther

I. INTRODUCTION

At high latitudes, especially around the Antarctic and Greenlandic coastlines, many glaciers terminate in the ocean. Depending on their behaviour sea-ward of the grounding line these glaciers terminate either as many of the tidewater glaciers around Greenland that have steep faces or, as common around Antarctica, as ice shelves, which have large floating ice tongues. It is the latter case that motivates the present study. Fresh water may flow out from the bed of a glacier at its grounding line due to in situ basal melting, especially if the ice is very thick, or due to surface melt, which can travel to the bed through englacial conduits and channels [1]. A considerable amount of glacially eroded sediment is also present at the bed and this is entrained into the basal meltwater and transported to the glacier front. The turbid mix of freshwater and sediment that emerges from under the glacier is typically less dense than the ambient seawater and so it rises along the underside of the ice shelf as a gravity current on a slope, which is referred to as a glacial meltwater plume [2, 3]. The typical slope of the underside of an ice shelf is on the order of one percent. And so, while the flow might be more accurately described as a gravity current, herein we describe the dynamics of flow under an ice shelf and under the shallow slopes in our laboratory experiments as a plume. The density of the particle-bearing plume changes as it advances as a consequence of the turbulent entrainment of seawater, the addition of meltwater and embedded sediments from the underside of the ice shelf and also due to the potential loss of particles that settle out of the plume and rain into the underlying ambient fluid. Depending upon the ambient stratification, the length of the slope and the particle sizes, the plume may eventually reach the surface or it may intrude into the ocean at a level of neutral buoyancy. The velocity, temperature and salinity of a glacial meltwater plume are used in determining the rate of melting (the "ablation velocity") of the glacier face. In models of glacier-ocean systems, the ablation velocity is typically parameterized as being proportional to the glacial meltwater plume velocity [4] and so it is crucial to model the evolution of the plume properly in order to make reliable predictions of ice sheet mass balance and, ultimately, of sea level rise. The idealized study presented here provides a starting point to examine the influence of particles upon the plume as well as the sedimentation patterns that result from the particles raining out of the plume.

Sedimentary records from fjords and beneath ice shelves contain information about ice sheet history [5]. However, detailed interpretation of these records requires a model linking sediment deposition to discharge conditions at the grounding line. In studies of particle-bearing gravity currents, many pertain to turbidity currents, which are more dense than the ambient fluid and which run down a slope [6]. These have been studied for their numerous environmental and industrial applications, for example, sediment laden rivers entering the ocean, submarine landslides, pyroclastic flows from volcanic explosions and avalanches. In these instances it is the particles that give the fluid negative buoyancy and drive the flow. As the flow evolves, entrainment of ambient fluid and settling of particles modify the buoyancy of the flow or remove it altogether [7–9]. Laboratory experiments of lock-release turbidity currents on a horizontal bottom have revealed non-trivial sediment deposition patterns that initially increase in depth from the lock and then gradually decrease to the distance of

run-out [7, 10]. A similar deposition pattern was observed in experiments of particle-laden gravity currents composed of fresh water and particles at sufficiently high concentration that the net current density was initially greater than the salt water ambient fluid into which it advanced [11, 12]. In this case, however, a local increase in sediment depth was observed just past the point of run-out because the interstitial fresh water then rose as a plume carrying some particles with it, and these eventually rained out to settle on the tank floor. By contrast, turbidity currents arising from a constant-flux source and moving over a horizontal bottom exhibited an approximately exponential decrease in sediment mass per area with distance from the source [10]. This is consistent with a model that assumes the particles are vertically well-mixed within a current whose height is approximately constant along its length.

The dynamics of glacial meltwater plumes are quite different from those of turbidity currents with or without reversing buoyancy. In this case, the particle-bearing plume is a mixture of fresh water and particles whose net density is less than that of the ambient fluid. As particles rain out of the plume, ostensibly this should increase the plume's buoyancy and hence its speed along the underside of an upward tilting slope. However, the descending particles can also carry some of the interstitial fluid with them, thus depleting the plume of buoyancy. In lock-release experiments of horizontally propagating particle-bearing fresh water gravity currents, the latter effect was found to dominate such that the currents came to a near halt as the particles descended [13].

For several reasons the pattern of particle deposition by glacial meltwater plumes is expected to be substantially different from that by turbidity currents. As particles settle from turbidity currents, they can create bedforms that act to guide the evolution of the current behind its head. Turbidity currents can also resuspend settled particles through shear stress on the bottom. A lofting turbidity current can result in deeper bedforms where the turbidity current stops. Furthermore, when moving downslope from a relatively shallow ambient fluid, entrainment into the turbidity current results in an ambient flow above the current which moves in the opposite direction to the current front. While this may impose additional drag on the current it does not act to advect particles upslope. By contrast, particles settling from a glacial meltwater plume cannot be resuspended by the plume and the resulting bedforms below the plume have no influence upon the propagation of the plume itself. However, the present study found for the first time that the entrainment-induced return flow of the underlying ambient fluid can carry settling particles back toward the plume source. Thus, whereas deeper bedforms develop near the stopping location of a lofting turbidity current, for glacial meltwater plumes deeper bedforms are anticipated closer to the source of the plume.

While there are some field observations of geological sediment patterns at the base of temperate glaciers [14], there are few laboratory measurements of sediment deposition resulting from particle-bearing buoyant plumes and gravity currents. In part, this is because of the difficulty in making accurate measurements when the maximum sediment depth may be on the order of a millimeter. One breakthrough in this regard is the development of a light attenuation method for measuring the depth of sediments composed of translucent particles [15]. This method was employed recently to examine sediment deposition from a

vertical particle-bearing plume in a uniformly stratified ambient fluid [16].

There have been some theoretical studies modelling sediment deposition by glacial meltwater plumes moving first near-horizontally as a jet, then rising vertically as a plume near a vertical ice face [17]. However, the case in which a buoyant, particle bearing plume flows up an inclined ceiling has not been previously studied either theoretically or by way of laboratory experiments. As such, this study addresses a big gap in understanding the effects of slope and particle properties on sediment distribution beneath a sloping "ice" face.

In §II we review standard theories for particle settling from turbidity currents and constant-flux particle bearing intrusions, these being adapted to particle-bearing plumes below an inclined slope. In §III we describe the setup of the experiments and analysis methods employed, with results presented in §IV. In §V we reconsider the standard theories for particle settling in light of the experimental observations. Conclusions are given in §VI.

II. THEORY

Here we focus on simple models for the depth of sediment arising from particle settling from a constant-flux buoyant plume with thickness $h_p(X)$ and (horizontal component of) velocity $U_x(X)$. As shown later in experiments, the particle-bearing fluid that is injected into the tank at $x = 0$ sets up a recirculation region from which the plume emerges at a distance x_r from the source. In developing the theory below, the dynamics of the recirculation region are ignored, with the focus being on the plume and particle-settling dynamics. Thus, for simplicity, we define the horizontal co-ordinate, $X \equiv x - x_r$, so that $X = 0$ corresponds to the location where the plume emerges from the recirculation region.

Generally, it is assumed that the flux of particles leaving the base of the plume is equal to the particle settling velocity, U_s, times the overlying concentration of particles within the plume. Conservation of particles requires that the difference in the volume flux of particles carried by the current between x and $x + dx$ is accounted for by the loss of the particles from the bottom of the current over the length dx. Thus we have

$$\frac{d}{dX}(U_x h_p \phi_p) = -U_s \phi_p, \tag{1}$$

in which ϕ_p is the concentration of particles by volume. The volume per unit width of particles settling below the plume over a length dX in time T while the system is in steady state is $dA_p = TU_s\phi_p dX$. If these particles consolidate directly below on the tank bottom with packing fraction p_f, the corresponding sediment depth, $h(X)$, is given by $p_f h dX = dA_p$. Hence,

$$h(X) = (1/p_f)TU_s\phi_p. \tag{2}$$

It is convenient to define a characteristic sediment depth to be

$$\bar{h} \equiv Q_{p0}T\phi_{p0}/(p_f\bar{\ell}), \tag{3}$$

in which Q_{p0} is the volume flux per unit width of fluid entering the plume and ϕ_{p0} is the particle concentration by volume in this fluid (see Fig. 1). The characteristic horizontal

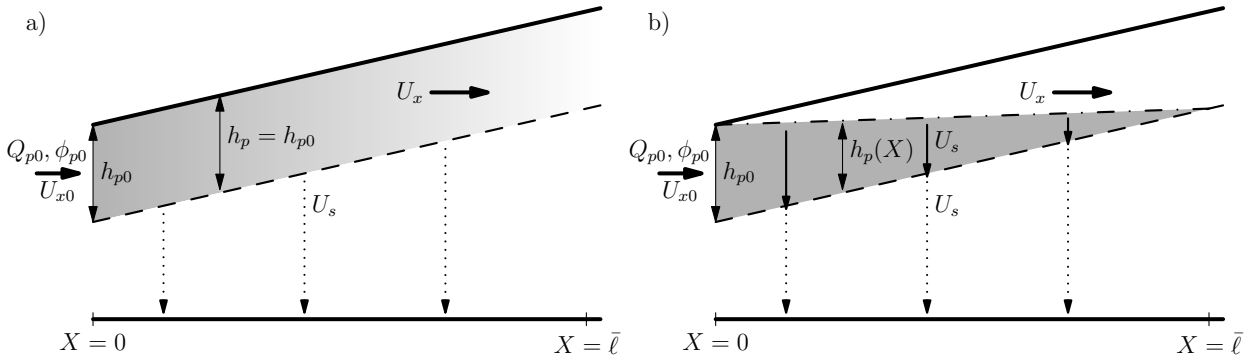

FIG. 1. Schematics illustrating particle settling from plumes in simple models with a) particles being vertically uniformly mixed across the plume and b) particles settling within the plume.

length scale for particles to rain out of the plume is denoted by $\bar{\ell}$. As such, $\bar{h}$ is the mean depth of sediments that consolidate on the bottom over a length $\bar{\ell}$ with packing fraction p_f resulting from a plume that flows for a time T. The value of $\bar{\ell}$ is estimated by assuming the particles leave the plume with a settling velocity U_s and the plume itself is assumed to have characteristic height h_{p0} and characteristic speed U_{x0}. Thus we define

$$\bar{\ell} \equiv h_{p0} U_{x0} / U_s = Q_{p0} / U_s. \tag{4}$$

From (2) and (3), the normalized sediment depth is

$$\frac{h(X)}{\bar{h}} = \frac{\phi_p(X)}{\phi_{p0}}. \tag{5}$$

We now consider two canonical models for particle settling from plumes, as illustrated in Fig. 1. A standard scenario for the study of constant-flux turbidity currents [10, 18, 19] assumes the particles are well mixed over the depth of the current, though entrainment of ambient fluid into the current is neglected. The current depth, h_p, and the current speed, U_x, are both assumed to be constant. This approach is straightforwardly adapted to particles raining out from a buoyant plume as in our experiments, as illustrated in Fig. 1a. Taking $U_x = U_{x0}$ and $h_p = h_{p0}$ to be constant in (1), we find

$$\phi_p(X) = \phi_{p0} \exp(-X/\bar{\ell}), \tag{6}$$

in which ϕ_{p0} is the particle concentration at the plume source and $\bar{\ell}$ is given by (4). Together with (5), this leads to the prediction that the normalized sediment depth decreases exponentially with distance from the source according to

$$h(X)/\bar{h} = \exp(-X/\bar{\ell}). \tag{7}$$

In a second scenario we adapt to the case of a plume model for settling-driven convection, in which particles settle from stationary fresh water into underlying stationary salt water [20–22], as illustrated in Fig. 1b. We assume that the plume has constant depth h_{p0} along its

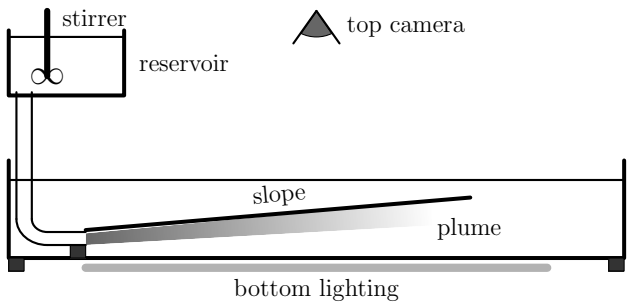

FIG. 2. Schematic of the experimental setup.

length when in steady state but that the particles settle at speed U_s within the plume. Implicitly this neglects turbulent entrainment into the plume and it assumes that a negligible volume of fluid is extracted from the plume by the particles that rain out of it. The particle concentration within the plume thereby remains constant over the length of the plume although the depth occupied by particles within the plume decreases linearly as $h_p(X) = h_{p0}[1 - X/\bar{\ell}]$ for $0 \le X \le \bar{\ell}$. Explicitly, the concentration of particles raining out from the bottom of the plume is

$$\phi_p(X) = \begin{cases} \phi_{p0} & 0 \le X \le \bar{\ell}, \\ 0 & X > \bar{\ell}. \end{cases} \tag{8}$$

Assuming the particles descend vertically below the plume, Eq. (5) suggests the sediment depth would be a constant, $\bar{h}$, over the distance $\bar{\ell}$ from the source.

III. EXPERIMENTAL SETUP AND ANALYSIS METHODS

The experiments were performed in a $L_T = 120.8\,\text{cm}$ long tank with height 18.5 cm and width $W_T = 4.5\,\text{cm}$, as illustrated in Fig. 2. The apparatus to generate the plume consisted of a reservoir whose bottom was suspended 1 m above the bottom of the tank. Clear tubing with $d_s = 0.8\,\text{cm}$ inner diameter emanated from a hole at the bottom of the reservoir. This passed through a valve and then through two sets of splitters such that the line-plume source in the tank consisted of four hoses spanning the width of the tank with a 0.8 cm high opening. With the valve closed, the reservoir was filled with 6 L of fresh water and a prescribed mass of ballotini (glass micro-spheres of density $2.5\,\text{g/cm}^3$ produced by MO-SCI Corporation) to give a target volume concentration of particles ϕ_0. The experiments used one of three types of particles with mean diameters (range) of $d_p = 45\,\mu\text{m}$ ($[38, 53]\,\mu\text{m}$), $64\,\mu\text{m}$ ($[53, 75]\,\mu\text{m}$) and $76\,\mu\text{m}$ ($[63, 90]\,\mu\text{m}$). These particles have predicted mean Stokes settling velocities of $U_s \simeq 0.15$, 0.31 and 0.44 cm/s, respectively. A stirrer in the reservoir ensured the particles were evenly distributed in suspension.

The line-plume source location in the tank was such that the opening rested upon a block of height, h_0, situated at a distance of 13 cm from the left-end of the tank. In typical experiments, $h_0 = 2.4\,\text{cm}$, although several experiments were performed with $h_0 = 4.0$, 6.5 and 9.0 cm. The tank was filled to a depth of 14 cm with salt water having density ρ_a

typically around $1.02\,\mathrm{g/cm^3}$, though in some cases being as large as $1.09\,\mathrm{g/cm^3}$. A modest exchange flow occurred between the fresh water already in the hoses (between the valve and the opening) and the salt water in the tank. The tank was then well mixed, and the density was accurately measured to $10^{-6}\,\mathrm{g/cm^3}$ accuracy with an Anton Paar DMA 5500 density meter.

A 88 cm long (and in one case with a slope angle $> 10°$, a 50 cm long) piece of acrylic having the same width as the tank was then inserted in the tank with one end resting just above the source opening and adjusted to have a constant slope rising upward and to the right of the source (Fig. 2). The acrylic was wrapped with foam tape to prevent any leakage between the slope and the tank walls. The preset slope was prescribed by its angle θ with the horizontal. In most cases $\theta = 4°$. However, experiments were performed with θ ranging between 0° and 10.3°. In all cases, the right-end of the slope was situated below the surface of the ambient fluid at least 20 cm from the right-end of the tank. Thus any fluid emanating from the plume at the outset would rise to the surface and partially move back over the top of the slope. This was designed so as to minimize the back-reaction of the plume fluid reaching the tank end wall and interacting again with the source.

With the slope in place, the valve was then opened allowing the plume fluid to flow freely from the reservoir into the tank under the slope. In different experiments the valve was opened to different degrees resulting in different volume fluxes. In all cases the valve was closed shortly before the reservoir emptied, denoting the end of the experiment. By recording the time that the valve was opened and recording the volume drained from the reservoir in that time, the volume flux Q_{00} was computed, having values ranging between 25 and $70\,\mathrm{cm^3/s}$. Dividing by the area of the source opening ($4\pi(d_s/2)^2$), the corresponding mean velocity of fluid leaving the source ranged approximately between 7 and 19 cm/s. Such high values helped ensure the particles remained in a turbulent suspension when passing through the hose from the reservoir to the source. The duration of the experiments ranged between 28 and 74 s.

Two analysis methods were employed to examine the experiments. In one, a side-view camera recorded the entire experiment from the time that the valve was opened to after it was closed and all the particles in the tank had settled to the tank floor. To aid in visualization, translucent mylar film was fastened to the rear side of the tank and lighting was provided by a LED lamp. For example, snapshots taken from a movie of one experiment are shown in Fig. 3. These clearly reveal the advance of the dark particles in the otherwise clear fluid of the plume. This experiment is typical of most experiments. Initially the fluid emanating from the line-plume source advanced rapidly as a momentum-driven turbulent jet (Fig. 3a). By entraining ambient fluid, the jet slowed its advance, and it gave rise to a circulation in the ambient fluid whereby fluid near the tank floor moved leftward toward the source so as to replace the fluid that was entrained into the jet. Thus a recirculating region develops extending between the slope and tank floor over a distance of approximately 16 cm from the source (Fig. 3b). Particles escaped from this recirculating region as part of the buoyant plume rising rightward along the slope. Particles continuously settled from the base of the particle-bearing plume into the underlying ambient fluid while being carried leftward back toward the recirculating region (Fig. 3c). As the particle-bearing plume continued to

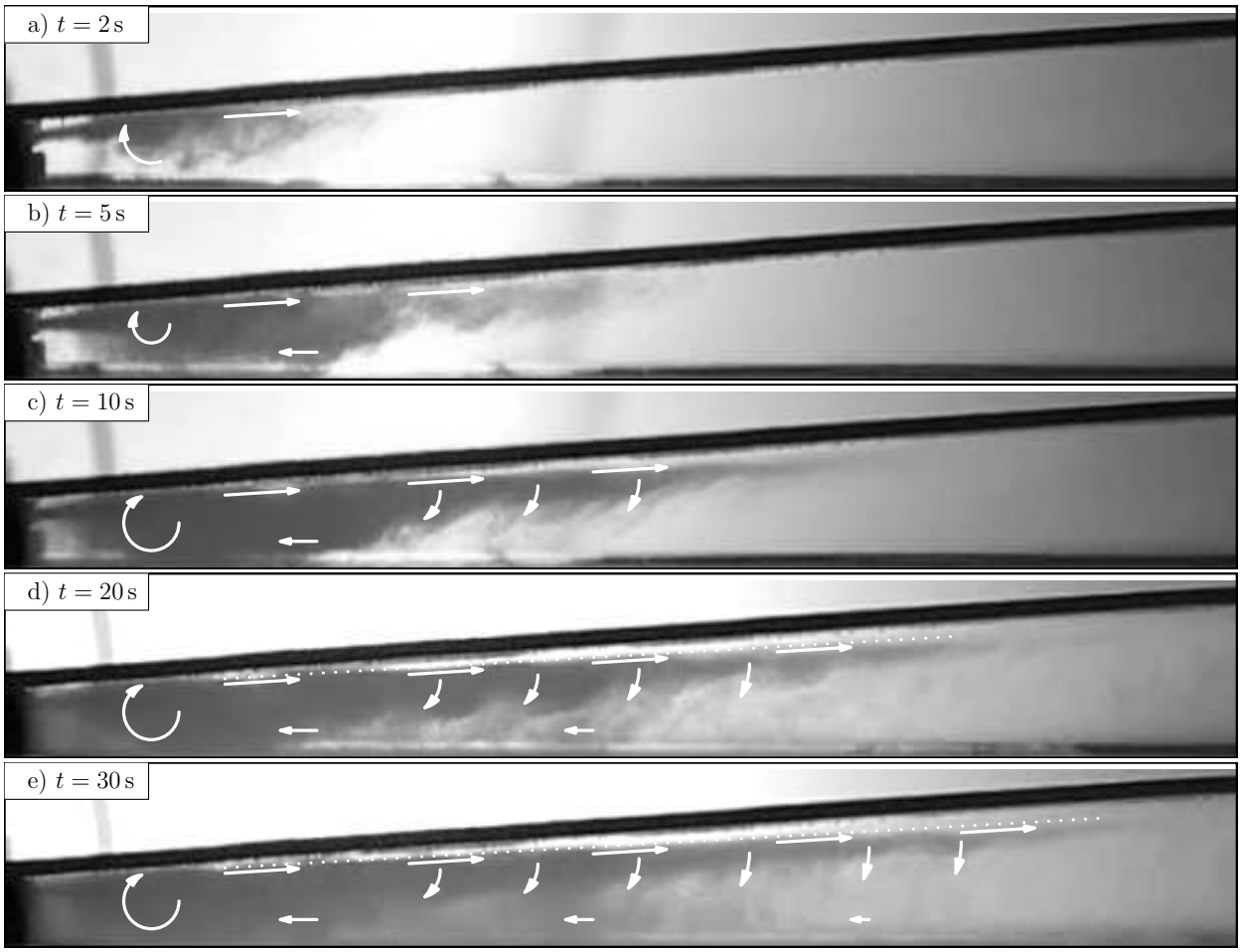

FIG. 3. [Multimedia online] Snapshots from Experiment 6 (with $\theta = 4°$, $d_p = 45\,\mu$m and $\phi_0 = 0.01$) showing the region extending 65 cm to the right of the source at 5 indicated times after the valve was opened. Superimposed white arrows qualitatively indicate the direction and speed of the flows. The dotted lines in d) and e) indicate the location of the settling front.

advance along the slope, the particles rained out through the plume fluid, as evident from the clear region between the slope and the right and upward-advancing particles (Fig. 3d). Indeed the slope of this settling front relative to the slope along which the plume propagates is comparable to the ratio of the Stokes settling speed to the speed of flow within the plume. This suggests that sufficiently far from the recirculating region and close to the slope, the plume is a laminar flow although measures of the speed and depth of the plume suggest typical Reynolds numbers on the order of 1000. Possibly this occurs because the descent of particles away from the slope inhibit turbulence near the boundary. In this experiment, by $t = 30\,\mathrm{s}$ the particles have nearly rained entirely out of the plume after travelling approximately 60 cm from the source (Fig. 3e). Far from the source, the particles fell nearly vertically downward and exhibited collective settling behaviour in which the descending particles fall in distinct lines rather than as a uniform cloud, as has been noted in previous experiments of particles in fresh water overlying salt water [13, 22, 23].

In order to extract quantitative information from the side-view movies, MatLab software was used to construct timeseries images, as shown in Fig. 4. Both time series were constructed by extracting slices through successive images in the movies and then vertically stacking these slices in time. The advance of the plume front along the slope and the collective motion of particles within this plume are examined by constructing a time series from diagonal slices through successive snapshots taken parallel to and 0.5 cm below the slope (Fig. 4a). The location of the plume front advancing along the slope close to the source was found from the leading advance of particles. Beyond this region, even if the particles fell out of the plume, the front between the remaining fresh water plume and salty ambient could still be visualized as a consequence of the difference in the indices of refraction of the two fluids. In all experiments, typically beyond 20 cm from the source, the front was found to advance at a near-constant speed. The x-component of the along-slope velocity was measured from the slope of the best-fit line through locations tracking the plume front between 20 and 40 cm from the source. The along-slope speed could then be computed by dividing by $\cos\theta$ in which θ is the angle of the slope from the horizontal. Generally the speed was found to be nearly constant in time with errors in the slope of the best-fit line being less than 10%. Typically in the diagonal time series, particle streaks behind the front had slopes, and therefore speeds, comparable to those of the front itself.

Time series were also constructed by stacking successive horizontal slices through images from movies, taken 1 cm above the bottom of the tank (Fig. 4b). These revealed the settling of particles, with particles farther from the source taking longer to reach the bottom of the tank. Also apparent from the tilt of streaks in these images is the existence of an ambient return flow that carried particles in the direction toward the source with the speed being larger closer to the source. The horizontal time series also reveals the recirculating region extending to about $16(\pm 2)$ cm from the source. Here the horizontal time series image is darker as a consequence of higher concentrations of particles that are advected directly by the recirculation from the slope to near the tank floor.

A separate analysis method is used to characterize the spatial pattern of particle deposition at the end of an experiment. The tank was lit underneath by a 80 cm square electroluminescent light sheet rotated nearly 45° with respect to the tank so that the length of the tank extended from one corner to the opposite corner of the light sheet. A second "top-view" camera situated 1.5 m above the tank was pointed vertically downward to view through the water free surface toward the light sheet. After the salt water was put in the tank the top-camera took a snapshot of the light sheet as viewed through the ambient water (Fig. 5a). The experiment then proceeded as described above. At the end of the experiment, when the particles in the tank had fully settled on to the tank floor, the slope was gently removed so as not to disturb the sediment bed. The camera then took a second picture of the light sheet whose intensity was diminished where particles had settled (Fig. 5b). The attenuation of light passing through the settled particles was made more clearly evident by constructing an image formed by pointwise dividing the pixel intensities of the final image from those in the initial image (Fig. 5c). Averaging across the span of the tank thus produced a plot of relative light intensity I_r versus distance x from the source.

Adapting the approach of Munro & Dalziel [15] and Sutherland & Dalziel [24], the relative

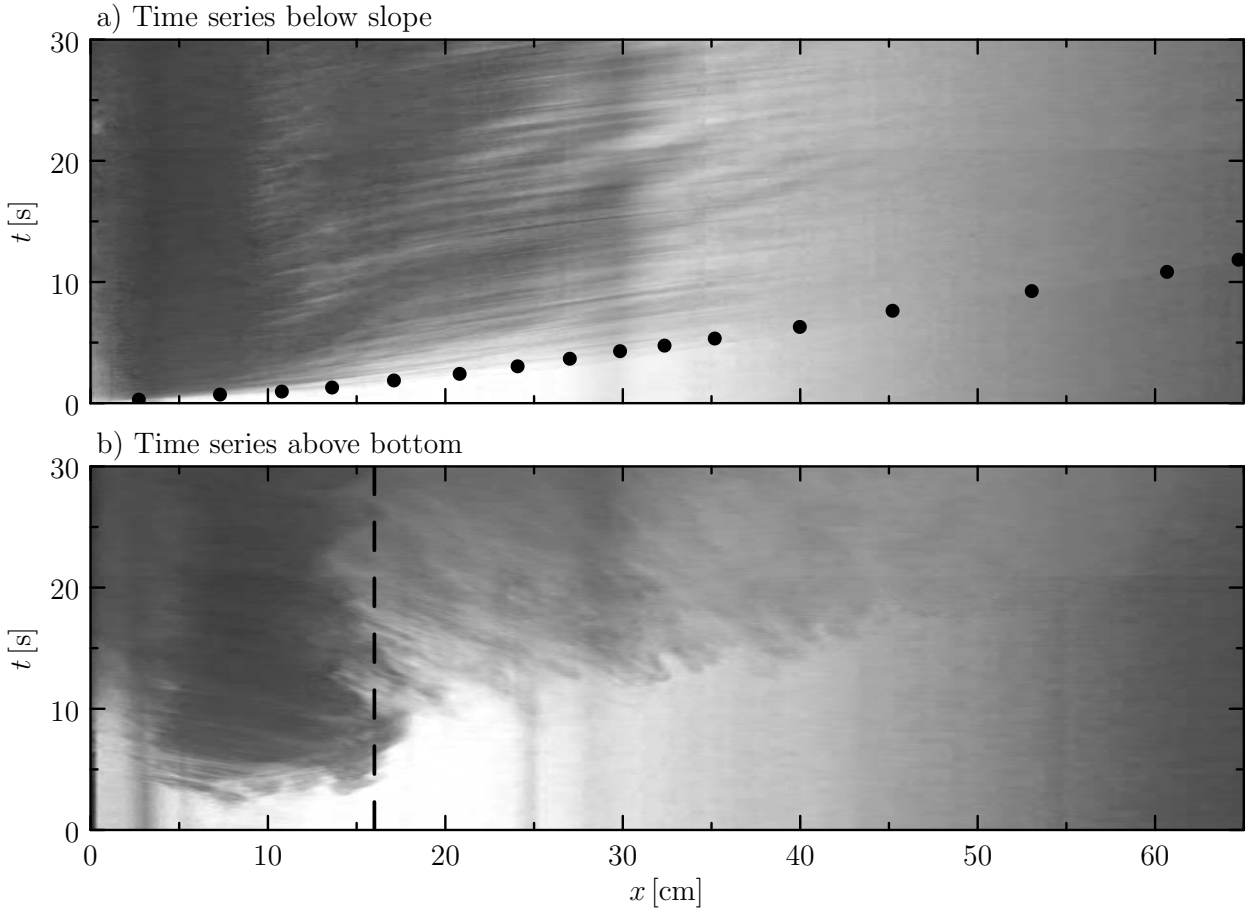

FIG. 4. Time series constructed from the sideview movie of the experiment shown in Fig. 3, a) constructed from slices parallel to and 0.5 cm below the slope and b) constructed from horizontal slices 1 cm above the bottom. The black dots in a) indicate points identified along the plume front advancing along the slope. The dashed black line in b) indicates the approximate maximum extent of the recirculating region.

intensity was used to infer the sediment depth by using a calibrating particle slope. To the side of the main tank, also over the light sheet, was situated a cubical calibration-tank measuring 18 cm on each side. This contained the same sized particles used in the experiments and was filled to 14 cm depth with the same density salt water as the ambient fluid in the tank. The particles at the bottom of the calibration tank were scraped to form a ramp having linearly increasing depth along its length. Averaging the light intensity across the width of the ramp thus produced a plot of intensity versus particle depth. Measurements of light passing through the particle-ramp showed the anticipated exponential decrease with particle depth, h, of light intensity, I_c, (relative to that with no particles) reaching the camera according to

$$I_c = I_b + (I_0 - I_b)\ e^{-h/\sigma}. \tag{9}$$

This involves three empirically measured quantities: I_b is the "black" intensity, I_0 is the

a) Top view before experiment

b) Top view at end of experiment

c) Ratio of final to initial intensity

FIG. 5. Top view images from Experiment 24 showing a) initial image, b) final image, and c) ratio of final to initial light intensities where the initial light intensity exceeds a minimum threshold, otherwise black. In all three cases the image extends between 5 cm and 75 cm in front of the source. Here, one corner of the square light sheet lies just in front of the source.

light intensity in the absence of particles and σ is the e-folding depth. The value of I_b was first estimated using the nonlinear regression routine "fitnlm" in MatLab. With this value, σ was found by performing a linear regression to find the best-fit line through a plot of h versus $\ln[(I_c - I_b)/(I_0 - I_b)]$. An example of the application of this method to determine the calibration formula (9) is shown in Fig. 6a.

The calibration formula is readily inverted so that from the measured intensity of light, $I(x)$, passing through the settled particles the depth of the sediment bed can be inferred, an example of which is shown in Fig. 6b. In practice, the depths measured within about 5 cm from the source were not reliable because either the corner of the electroluminescent light sheet did not extend across the full span of the tank and/or because the particle depth was so large due to the recirculating flow that the intensity of light passing through the particles was effectively black.

In all, 25 experiments were performed and analyzed with the intent to characterize the pattern of particle deposition primarily as it depends upon slope angle θ, particle volume concentration, ϕ_0, and particle diameter, d_p. These as well as other input parameters and measured quantities for all experiments are listed in Table I.

IV. EXPERIMENTAL RESULTS

A. Qualitative Observations

As discussed above regarding Fig. 3, the experiments generally showed a plume propagating along the slope carrying particles that eventually rained out of the plume. As the particles settled towards the bottom of the tank, they were advected back towards the source

Exp.	H_0	θ	d_p	ϕ_0	Q_{00}	T	ρ_a	ρ_0	F_0	U_x	x_r	$1000S_h$	h_{s0}
1	10.1	0.0	45	0.010	36.6	58	1.020	1.012	270.8	4.4	15	-	-
2	10.3	2.0	45	0.010	28.0	58	1.021	1.012	228.2	5.5	-	1.1	0.12
3	7.1	2.0	45	0.010	52.8	45	1.021	1.012	411.3	4.5	-	0.6	0.17
4	7.5	3.8	45	0.010	32.8	59	1.022	1.012	303.0	6.1	7	-	-
5	5.1	3.9	45	0.010	41.2	47	1.022	1.012	378.6	-	-	1.6	0.19
6	3.6	4.0	45	0.011	32.8	59	1.018	1.013	151.4	5.1	16	3.5	0.28
7	3.2	4.0	45	0.010	36.5	65	1.021	1.012	305.2	5.3	12	2.5	0.31
8	3.6	4.0	45	0.010	53.0	33	1.062	1.012	2430	10.9	-	-	-
9	3.6	4.0	45	0.010	59.2	38	1.090	1.012	4154	13.5	21	-	-
10	3.9	4.3	45	0.050	26.6	61	1.079	1.067	269.3	9.5	-	10.2	0.79
11	3.2	6.3	45	0.010	51.5	34	1.022	1.012	452.5	6.0	16	-	-
12	3.6	6.4	45	0.010	53.6	42	1.022	1.012	468.2	4.4	17	2.4	0.27
13	3.6	10.3	45	0.010	49.7	44	1.022	1.012	447.0	5.7	14	1.3	0.15
14	10.2	2.0	64	0.010	41.2	47	1.021	1.012	356.4	-	-	2.0	0.23
15	3.6	3.9	64	0.030	54.7	48	1.049	1.040	427.4	8.0	20	20.0	1.28
16	3.6	4.0	64	0.021	45.3	40	1.036	1.027	362.6	7.9	15	5.6	0.36
17	3.6	4.0	64	0.030	56.3	40	1.051	1.040	563.8	8.2	24	13.7	0.88
18	3.9	4.1	64	0.010	45.3	40	1.021	1.012	377.3	5.0	18	3.3	0.21
19	3.6	4.5	64	0.010	30.5	41	1.020	1.012	221.3	6.8	16	4.5	0.26
20	3.5	5.8	64	0.010	31.3	74	1.022	1.011	314.7	4.4	15	7.7	0.46
21	3.5	6.4	64	0.010	28.9	54	1.020	1.012	215.5	5.9	-	-	-
22	10.3	1.9	76	0.010	71.4	28	1.022	1.012	649.5	-	-	2.1	0.19
23	10.3	2.1	76	0.010	25.6	78	1.022	1.012	234.9	3.8	-	3.5	0.18
24	3.5	4.0	76	0.010	51.4	45	1.021	1.012	417.6	5.3	18	5.3	0.33
25	3.5	6.3	76	0.010	32.4	54	1.021	1.012	278.5	6.1	17	3.2	0.21

TABLE I. Input and relevant measured quantities for the experiments reported upon here. All values are given in cgs units except for the particle diameter. Explicitly, input parameters are the height of the top of the line-plume source above the tank bottom H_0 (cm), the angle of the slope θ (degrees), the mean particle diameter d_p (μm), the particle volume concentration at the source ϕ_0, the source volume flux Q_{00} (cm^3/s), the experiment duration T (s), and the ambient fluid density ρ_a (g/cm^3). Also given are the computed source density ρ_0 (g/cm^3) and buoyancy flux per unit width F_0 (cm^3/s^3) as well as the measured horizontal component of the plume velocity U_x (cm/s), the extent of the recirculating region x_r (cm), 1000 times the magnitude of the sediment slope S_h, and the extrapolated sediment depth at the source h_{s0} (cm). Values are given to the accuracy of the measurement error except for the ambient density which is measured to 6-digit accuracy. The dashes indicate values that could not be measured.

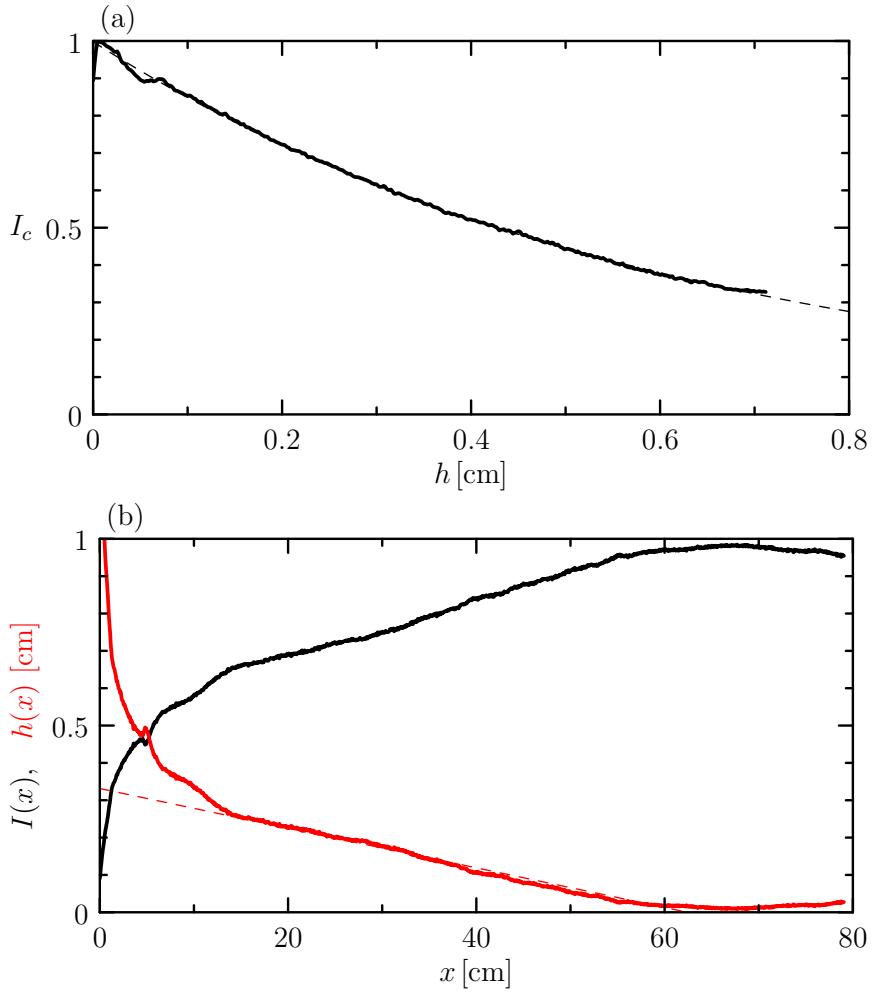

FIG. 6. [Color online] a) Relative light intensity versus particle depth measured from the calibration particle-ramp (black) and the best-fit exponential (dashed) given by (9) with $I_0 = 0.998 \pm 0.091$, $I_b = 0.0083 \pm 0.0113$ and $\sigma = 0.611 \pm 0.001$. b) Measured relative light intensity (black) and sediment depth (solid red) versus distance from the source from Experiment 24. The dashed red line shows the best-fit line through the sediment depth data for $20\,\text{cm} \leq x \leq 50\,\text{cm}$.

before either being deposited at the base of the tank or re-entering the strong recirculating region that extended between 10 and 20 cm from the source, depending upon the flow parameters. While these qualitative features were observed in all experiments, some aspects varied depending upon the experiment parameters.

In experiments with larger diameter particles, the particles were always observed to settle out of the plume before reaching the end of the slope. In some experiments with very small particles having mean diameter $20\,\mu$m (not examined here), the particles remained entirely suspended in the plume even as it reached the end of the slope and the tank end-wall.

In experiments with the source raised higher above the tank floor ($H_0 \gtrsim 8\,\text{cm}$), with low volume fluxes ($Q_{00} \lesssim 30\,\text{cm}^3/\text{s}$) or with very saline ambient fluid ($\rho_a \gtrsim 1.06\,\text{g/cm}^3$), the ambient fluid below the plume still propagated toward the source but the recirculating

region was not so pronounced.

For the slope angles examined in this study, the slope angle did not have a significant effect upon the flow. Even in experiments for which the slope was horizontal, the plume advanced from the recirculating region to the end of the slope with particle-settling through the plume being evident.

B. Quantitative Observations

As a step toward predicting the pattern of sediment deposition from a particle-bearing plume rising along a slope, it is important to determine the speed at which the plume propagates along the slope. As discussed above, the x-component of the along-slope velocity, U_x, was measured from time series constructed from diagonal slices 0.5 cm below the slope (e.g. see Fig. 4a). The along-slope speed was then estimated to be $U_p = U_x/\cos\theta$, in which θ is the known slope angle.

Several factors are expected to influence the speed of the plume away from the recirculating region with the most important being the buoyancy flux. Because the particle concentrations were small (with $\phi_0 \simeq 0.01$ in most experiments and ϕ_0 no greater than 0.03), the plume speed is expected to be determined primarily by the buoyancy flux, F, of the plume neglecting the change in buoyancy due to settling particles. The buoyancy flux of the plume that emerged from the recirculating region is expected to be related to the buoyancy flux associated with the fluid leaving the line-plume source,

$$F_0 = g_0{}'Q_0, \tag{10}$$

in which $Q_0 \equiv Q_{00}/W_T$ is the volume flux per unit width of the tank,

$$g_0{}' = g(\rho_a - \rho_0)/\rho_a \tag{11}$$

is the reduced gravity of the source fluid with respect to the ambient fluid, and $\rho_0 = \rho_p\phi_0 + \rho_{00}(1-\phi_0)$ is the density of the fluid leaving the source, composed of fresh water with density $\rho_{00} = 0.9982\,\mathrm{g/cm^3}$ and particles of density $\rho_p = 2.5\,\mathrm{g/cm^3}$. Although the source fluid mixes with the ambient fluid within the recirculating region before rising up the slope as a plume, the buoyancy flux is conserved. Thus, following Britter & Linden [25], we expect the along-slope speed of the plume to be proportional to $F_0^{1/3}$.

Figure 7 plots the observed front speed versus the value of $F_0^{1/3}$ for all the experiments in this study. There is some scatter in the data for experiments with moderate values of ambient density ($\rho_a \simeq 1.02\,\mathrm{g/cm^3}$), which can be attributed to the details of the dynamics within the recirculating region, which itself depends upon H_0, Q_{00} and ρ_a. However, when including experiments with very saline ambient water (for which $F_0^{1/3} > 10\,\mathrm{cm/s}$), it seems reasonable to suppose that the relative buoyancy of the plume and ambient water is the driver of the observed dynamics. The best-fit line through the data that passes through the origin gives the relationship for the plume front speed of

$$U_x = 0.85(\pm 0.04)F_0^{1/3}. \tag{12}$$

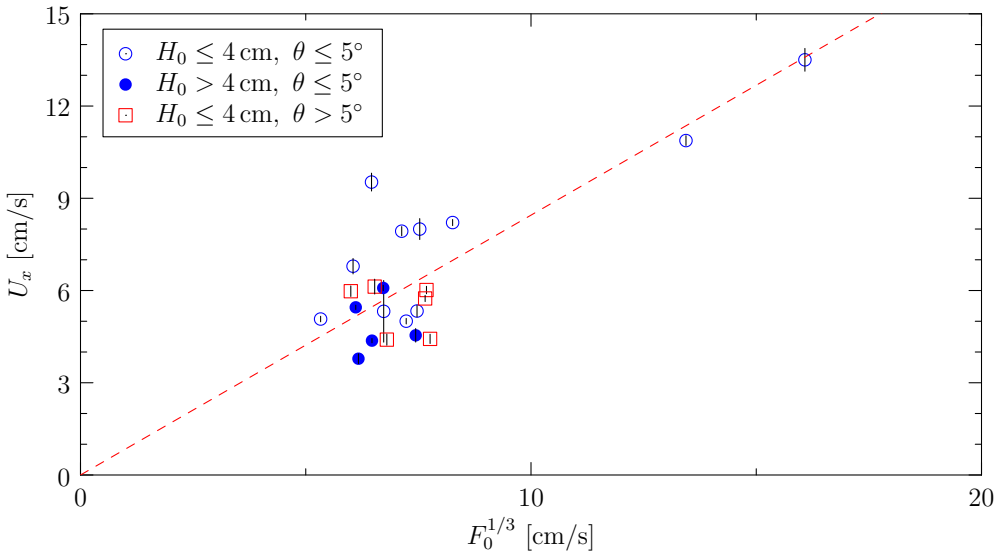

FIG. 7. [Color online] Observed plume front speed compared with the predicted theoretical value.

The coefficient of proportionality is smaller than the value 1.5 determined by Britter & Linden [25]. This can be attributed to several factors depending upon the experiment parameters including the influence of the strong underlying return flow into the recirculating region and the lack of significant turbulent entrainment into the plume far from the recirculating region because the descending particles act against the momentum of the rightward rising plume.

In all experiments, the sediment depth was found to decrease almost linearly with distance from the plume source within a range extending beyond the recirculating region. Because different experiments were performed with different source particle concentrations, ϕ_0, and with source fluid injections occurring for shorter or longer times T depending upon the volume flux $Q_{00} = Q_0 W_T$, it is convenient for comparison purposes to normalize the measured sediment depth by $\bar{h}$, defined by (3), and the horizontal position by $\bar{\ell}$, defined by (4). We use externally controlled experimental parameters (see Table I) to define these characteristic scales, with the characteristic plume speed and height given by

$$U_{x0} \sim {F_0}^{1/3}, \quad \text{and} \quad h_{p0} \sim H_0/2, \tag{13}$$

respectively. The scaling for the plume height, being approximately half the domain height at the source, is consistent with observations of experiments in which a recirculation region forms (e.g. see Fig. 3b), and is chosen to conform with the theory for full-depth lock-release gravity currents whose height upon release is half the domain height. Thus the volume flux per unit width into the plume is $Q_{p0} = U_{x0} h_{p0}$. The particle concentration by volume entering the plume is assumed to equal the particle concentration at the source: $\phi_{p0} = \phi_0$. The packing fraction is taken to be $p_f = 0.56$, corresponding to the loose packing of spheres. It should be emphasized that the estimates for $\bar{h}$ and $\bar{\ell}$ using (13) and $\phi_{p0} = \phi_0$ are somewhat crude: the observed plume front speed, shown in Fig. 7 shows significant variability, particularly for $6\,\mathrm{cm/s} \lesssim F_0^{1/3} \lesssim 8\,\mathrm{cm/s}$; the depth of the plume emerging from

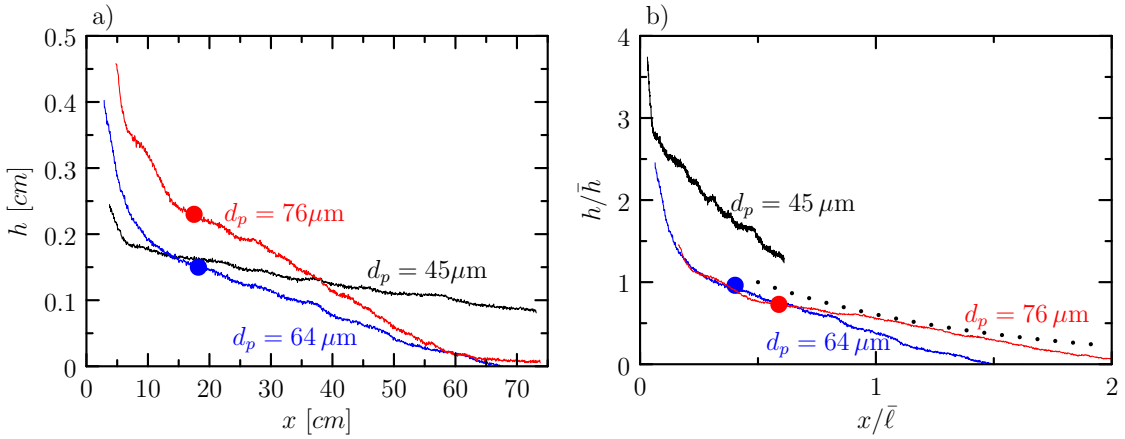

FIG. 8. [Color online] a) Sediment depth with distance from source for experiments with $\phi_0 = 0.01$, $\theta = 4°$ and different particle diameters as indicated for Experiments 5, 18 and 24. b) Same data but normalized. The superimposed circles indicate the observed maximum extent of the recirculating region. In b), the dotted curve represents the exponential given by (7) with $X = x - x_r$ and normalized extent of the recirculation region taken to be $x_r/\bar{\ell} = 0.5$.

the recirculation region is difficult to observe after the particles begin settling; and the particle concentration entering the plume is likely modified by particle settling within the recirculation region and by recycling of particles into the plume that enter through the return flow underlying the plume. Nonetheless, the use of these scalings are useful in providing comparisons of sediment depth profiles between experiments.

The variation of the sediment depth with distance from the line-plume source as it depends upon the particle diameter in three experiments is shown in Fig. 8. As anticipated, the smaller diameter particles, which have a slower Stokes settling velocity, are distributed more broadly over the horizontal extent of the tank. While the decrease in sediment depth is nearly linear in all three cases for $20\,\text{cm} \lesssim x \lesssim 50\,\text{cm}$, the magnitude of the sediment slope is steeper in experiments with larger diameter particles. In particular, in the case with $d_p = 76\,\mu\text{m}$, nearly all of the particles had rained out within approximately 70 cm of the source and the depth of the particles closer to the source was much higher. When the depth and distance are scaled by $\bar{h}$ and $\bar{\ell}$, respectively, there is a good collapse of data for the moderate and large particles (Fig. 8b). The experiment with the smallest particles had smaller source volume flux Q_{00} and larger source depth H_0. Consequently, no significant recirculation region was evident in this case, which may explain why this curve does not collapse upon the curves with the larger particles since the recirculation acts significantly to change the particle concentration and volume flux from the source to that exiting the recirculation region and entering the plume.

The effect of particle concentration upon sediment deposition had only moderate influence upon the (normalized) sediment deposition pattern, as shown in Fig. 9. In all three cases, a recirculation region extended between 15 and 20 cm and the data collapse reasonably well when scaled by $\bar{h}$ and $\bar{\ell}$.

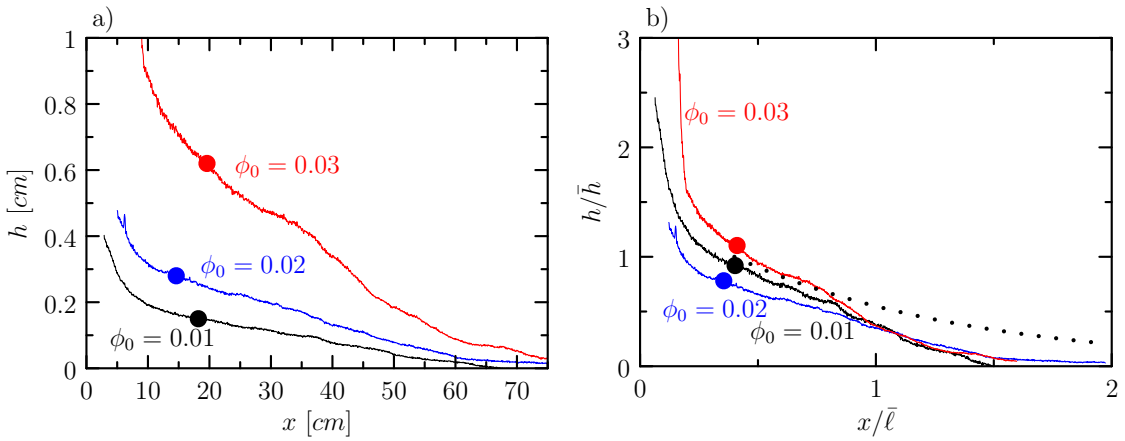

FIG. 9. [Color online] As in Fig. 8 showing the normalized sediment depth with distance from source for experiments with $d_p = 64\,\mu$m, $\theta = 4°$ and different particle concentrations as indicated for Experiments 16, 17 and 18. In plotting (7) by the dotted line, the normalized extent of the recirculation region taken to be $x_r/\bar{\ell} = 0.4$.

The angle of the slope had only a moderate influence on the (unnormalized) sediment slope, as shown in Fig. 10. The decrease of sediment depth with distance from the source was nearly the same in all experiments. However, when the height and length are scaled against $\bar{h}$ and $\bar{\ell}$, respectively, only the cases with $\theta = 3.9°$ and $\theta = 6.4°$ collapse well (Fig. 10b). The case with $\theta = 2.0°$ had source depth $H_0 = 10.3\,$cm, and no recirculation region was observed. In the case with $\theta = 10.3°$, $H_0 = 3.6\,$cm and a recirculation region was evident. However, the steeper slope resulted in less turbulent mixing between the plume and the deeper underlying return flow far from the recirculation region. This suggests that the normalized sediment profile was shallower in this case because of less effective detrainment of particles from the plume by turbulent processes; away from the recirculation region, particles rained out from a relatively laminar plume.

In the right plots of Figs. 8-10, the dotted line shows the normalized sediment depth profile predicted by (7) in which $X = 0$ corresponds to the location where the plume emerges from the recirculation region (at $x = x_r$). The theory leading to (7) assumed the plume was turbulently well-mixed over its depth an that particles settled vertically downward below the bottom of the plume. The theory neglected the observed dynamics of the return flow that acts to carry particles back toward the recirculation and which enhances turbulence between the plume and the underlying ambient fluid. The neglect of these processes leads to the prediction of an exponentially decreasing sediment depth. Whereas the observations show that the sediment depth decreases approximately linearly with distance below the plume.

If h and x were properly normalized by $\bar{h}$ and $\bar{\ell}$, respectively, one should expect the normalized volume of sediment per unit width to be

$$\bar{A} \equiv \int_0^\infty h\,dx/(\bar{h}\bar{\ell}) \simeq 1, \tag{14}$$

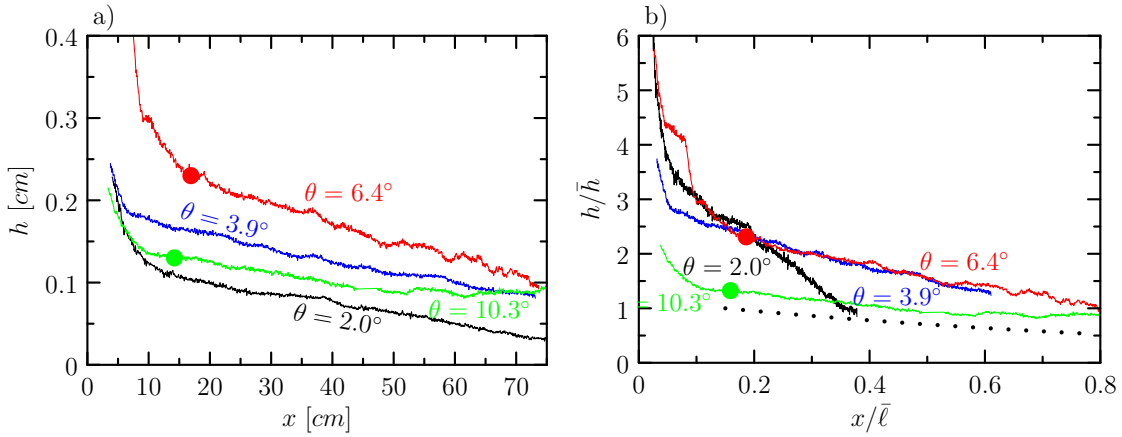

FIG. 10. [Color online] As in Fig. 8 showing the normalized sediment depth with distance from source for experiments with $\phi_0 = 0.01$, $d_p = 45\,\mu$m and different angled slopes as indicated for Experiments 2, 5, 12 and 13. In plotting (7) by the dotted line, the normalized extent of the recirculation region taken to be $x_r/\bar{\ell} = 0.15$.

And so, over the range where the sediment depth was measured, the volume per unit width should be at most unity, with the remainder being accounted for by particles that settle in the recirculation region. This is the case for experiments with $d_p = 64\,\mu$m and 76 mum in Fig. 8, for all the experiments in Fig. 9, but for none of the experiments in Fig. 10. This suggests that experiments with $\bar{A} > 1$ are not properly normalized by the choice of $\bar{h}$ and $\bar{\ell}$, due to the heuristic choice of the velocity and length scales estimated by (13) and the assumption that $\phi_{p0} = \phi_0$.

Although a qualitative pattern is revealed in these three examinations of the normalized sediment depth profiles, $h(x)/\bar{h}$, a quantitative picture is more difficult to discern. In an attempt to create a holistic representation of all the experiments, the structure of the sediment bed was classified in terms of the properties of the best-fit line through $h(x)$ for 20 cm $\leq x \leq 50$ cm. The magnitude of the slope of the line gives the slope, S_h, of the sediment bed sufficiently far from the recirculating region and the intercept of the line with $x = 0$ gives a measure of the depth, h_{s0}, the bed would have at the location of the source. In reality, the actual depth of sediment near the source was observed to be at least twice as large due to the accumulation of particles in the recirculating region.

The values of h_{s0} and S_h are plotted in Fig. 11. To account for the difference in the volume of injected particles between different experiments, h_{s0} is normalized by twice the characteristic height $2\bar{h}$, with $\bar{h}$ given by (3). Likewise the slope is normalized by $2\bar{h}/\bar{\ell}$, which is the slope the bed would have if decreasing linearly from depth $2\bar{h}$ at the source to zero depth at the characteristic distance ℓ. (Consistently, such a sloping sediment bed has mean depth $\bar{h}$.)

The data exhibit an approximate linear increase in normalized depth $h_{s0}/(2\bar{h})$ with normalized slope $S_h/(2\bar{h}/\bar{\ell})$, particularly for the experiments in which a recirculation region was evident (as indicated by the open symbols). The four experiments for which the slope is

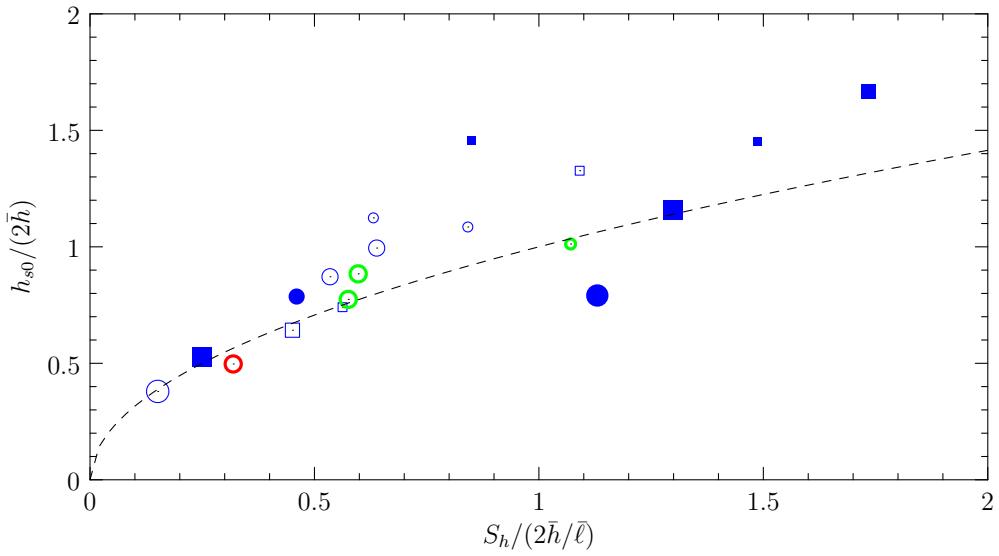

FIG. 11. [Color online] Normalized sediment depth extrapolated to $x = 0$ versus normalized sediment slope for a range of experiments as indicated by the different symbols. Symbol size indicates particle size (small 45 μm, medium 64 μm, large 76 μm), colour denotes particle concentration (blue $\simeq 0.01$, red $\simeq 0.02$, green $\gtrsim 0.03$), shape denotes source volume flux (circle $Q_{00} < 40\,\mathrm{cm}^3/\mathrm{s}$, square $Q_{00} > 40\,\mathrm{cm}^3/\mathrm{s}$), symbols are open if a recirculating region develops near the source and are closed otherwise. The dashed line denotes values of h_{s0} and S_h for which the volume per unit width of sediment equals $\bar{h}\bar{\ell}$.

largest, all correspond to experiments in which no recirculation region was evident. However, three experiments with no apparent recirculation region also have smaller slopes and depths that are comparable to those for experiments with a recirculating region. As stated above, the scalings used to normalize h_{s0} and S_h, according to (3) and (4) with (13), were somewhat heuristically chosen to depend upon explicitly determined experimental parameters. With an appropriate choice of $\bar{h}$ and $\bar{\ell}$, the volume per unit width of sediment should be no larger than $\bar{A} = \bar{h}\bar{\ell}$. The values of h_{s0} versus S_h for which the volume per unit width, $h_{s0}^2/(2S_h)$, equals $\bar{A}$ is plotted as the dashed line in Fig. 11. While this curve passes through the data points, it underlies several of the data points indicating that the estimates for $\bar{h}$ and $\bar{\ell}$ for these experiments under-predict the volume per unit width of the sediment depth.

This analysis suggests that, while the scalings crudely capture order of magnitude estimates of the sediment depth and slope, other dynamics not captured by $\bar{h}$ and $\bar{\ell}$ influence sediment deposition. Below we discuss in more detail the processes neglected in formulating these scalings through the simple theories presented in § II, taking into account experimental observations.

V. DISCUSSION

If the simple model, illustrated in Fig. 1a, captured the full dynamics of the experiments, then the sediment depth profiles in Figs. 8-9 would collapse onto a single curve representative of an exponential function, and the normalized depths and slopes plotted in Fig. 11 would collapse onto a single point. However, the snapshots in Fig. 3, show that additional processes occur that non-negligibly affect the ultimate pattern of sediment deposition from the plume.

The transient effects associated with the start of injection and with particle settling after the source is turned off cannot explain the observed deposition pattern. When it occurs, a recirculation region forms in less than 5 seconds in all experiments and the typical time for the particles to rain out of the plume is less than 10 seconds. With a typical injection time of about 50 seconds, this suggests that 80% to 90% of the particles are injected while the system is in quasi-steady state.

The schematic in Fig. 12 illustrates the essential processes thought to be taking place in the transport and deposition of sediments by a buoyant plume rising beneath a model ice shelf in our experiments. The particle-bearing flow entering the domain on the left consists of a mixture of fresh water and particles such that the mixture has a total density smaller than that of the ambient fluid even though the particles have density larger than the ambient fluid. The forced (initially momentum-driven) line plume at the source is assumed to be spanwise uniform so that the source volume flux may be characterized by Q_0, the volume per time per unit width of the domain. The forced line plume enters the domain at a height between $z = h_0$ and H_0. The domain itself has a trapezoidal cross-section with a horizontal lower boundary at $z = 0$ and a sloping upper boundary at $z = H(x) = H_0 + sx$, in which $s = \tan\theta$ and θ is the angle the upper boundary forms with the horizontal.

One reason for the spread of the normalized depths and slopes in Fig. 11 is the presence of the recirculation region which lowers the particle concentration at the source from its presumed value of ϕ_0 and which increases the volume flux into the plume, Q_{p0}, from the source volume flux, Q_0, due to entrainment of the volume flux Q_{r0} associated with the return flow. The depth of the plume where it exits the recirculating region, at $x = x_r$, is not well defined, particularly if the return flow interacts strongly with the plume resulting in a turbulent shear flow. This adverse momentum can also have an influence on the propagation speed of the plume at least near x_r. Hence the explicit experimental parameters used to define the normalization scales, $\bar{h}$ and $\bar{\ell}$, are imprecisely determined because they do not take into account the change in volume flux and particle concentration due to the recirculation region.

Furthermore, while one might argue that the profiles are approximately exponential, the assumptions of a well-mixed current of constant depth is not consistent with observations that show a settling front of particles within the current and a finite distance, x_F, beyond which the plume is devoid of particles (Fig. 3). The observation of a settling front within the plume is consistent with the simple model illustrated by Fig. 1b. However, that model predicted that the underlying sediment depth would be constant, not decreasing to zero, as observed in experiments. An extension to the simple theoretical models in § II includes the motion of the ambient fluid underlying the particle-bearing plume that flows back toward the

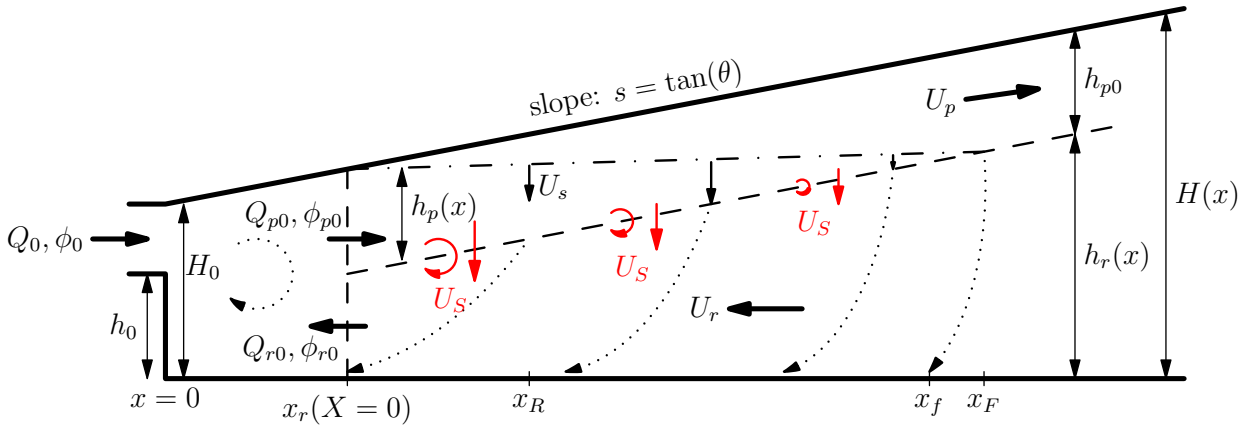

FIG. 12. [Color online] Schematic showing essential processes and variable definitions for sediment transport and deposition. Double arrows indicate heights, single solid-arrows indicate velocities, single dotted-arrows indicate particle paths, the curved red arrows represent mixing between the plume and return flow, and the downward red arrows represent the enhanced settling velocity resulting from turbulent detrainment of particles. The recirculating region lies to the left of x_r. The plume of constant depth h_{p0} runs up the slope with speed $U_p = U_x/\cos\theta$, having the lower boundary indicated by the dashed line. Particles near the top of the plume at the settling front (dashed-dotted line) settle at the Stokes settling speed, U_s. Turbulent detrainment leads to enhanced settling at speed $U_S(x)$ across the interface between the plume and underlying return flow (diagonal dashed line). Below the plume particles settle over a vertical distance $h_r(x)$ while being swept leftward at speed $U_r(x)$ toward the recirculating region. Particles leaving the plume between $x = x_r$ and x_R are carried back into the recirculating region. The furthest distance at which particles settle on the tank bottom is x_f.

recirculation region (Fig. 12). Thus particles raining out from the plume's base are carried leftward by the return flow as they descend. While some of these particles may approach the bottom of the tank, those between x_r and x_R are carried into the recirculating region where they are partially recycled back into the plume and partially settle out. It is possible that particles reaching the bottom at $x > x_R$ may be transported into the recirculating region through bedload transport by the return flow, although this was difficult to observe directly during the experiments. Again assuming the plume depth, h_{p0}, is constant, the underlying return flow, U_r, must increase leftward the closer it is to the recirculation region. This follows from volume conservation, so that $h_r U_r = h_{p0} U_x$, and the geometric constraint $h_r + h_{p0} = H_0 + sx$. Hence,

$$U_r(x) = h_{p0} U_x / (H_0 - h_{p0} + sx). \tag{15}$$

Such a horizontally divergent flow beneath the region of the plume where a settling front is observed would result in a sediment depth that would increase with distance from the source, counter to what is observed.

Another extension to the simple models includes the effect of entrainment into the particle-bearing plume. In this case the depth of the plume increases with distance from the

recirculation region although the underlying ambient fluid depth still increases with distance from the recirculation region. However, in steady state, entrainment acts to carry particles in the underlying return flow back into the plume. Assuming there is no difference in the particle concentration within the plume and within the underlying fluid, the particle concentration in the plume is unchanged by entrainment. That said, the turbulent interaction between the plume and the return flow does have an effect on particle deposition that is different from that for turbidity currents. For the latter, particles rain out into a relatively laminar bottom boundary layer where they settle. For the case of a plume, the underlying turbulence acts to detrain particles at a rate faster than the Stokes settling velocity. This is illustrated by the red arrows in Fig. 12. As illustrated by (15), the shear between the plume and the return flow is largest near the plume source and this induces larger mixing between the plume and return flow in this region, as can be inferred from Fig. 3. Further away from the source the shear is weaker and hence less mixing occurs. This suggests that mixing results in the detrainment of particles from the plume which can be characterized by an enhanced settling speed, $U_S(x)$, across the interface between the plume and underlying return flow, which we refer to as the "detrainment speed". By analogy with (2) and (5), the resulting normalized depth of sediment is given by

$$\frac{h(x)}{\bar{h}} = \frac{\phi_p(x)}{\phi_{p0}} \frac{U_S(x)}{U_s} \tag{16}$$

The spatial variation of U_s together with the variation of turbulent mixing within the plume and the effect of the settling particles being carried with horizontally varying speeds toward the source all contribute to the pattern of sediment deposition, and the complex dynamics of the recirculation region is also crucial for setting the plume source conditions. While our experiments were not designed to examine these processes in detail, they have served to elucidate the essential dynamics that should be investigated further in order to understand sediment deposition below a glacier meltwater plume.

VI. CONCLUSIONS

We have performed laboratory experiments examining the transport of particles by a buoyant plume rising up a uniform shallow slope. Near the source a recirculating region formed if the momentum of the injected fluid is relatively large and the source not too elevated from the floor of the tank. While enhanced particle deposition occurred in the recirculating region, some particles were carried away by the plume that was observed to propagate at near-constant speed along the rising slope. At least close to the sloping upper boundary the plume was laminar, as indicated by the observation that particles within the plume settled at the Stokes settling velocity while being carried up-slope along with the plume. The particles eventually rained out of the plume and, while settling through the underlying flow, were transported in the direction of the source before settling. The sediment depth beyond the recirculating region decreased approximately linearly with distance from this region. This suggests that turbulent processes between the plume and the underlying return flow resulted in a change of particle concentration, ϕ_p, and detrainment of particles

from the plume at speeds, $\tilde{U}_S$, such that $\phi_p \tilde{U}_S$ decreases approximately linearly with distance from the recirculating region, although this could not be measured directly.

Generally, the magnitude of the sediment slope was larger in experiments with larger particles though the dependence of sediment slope upon the slope of the upper boundary and particle concentration was less straightforward due to the complicated turbulent processes in the recirculation region. However, the experiments do reveal dynamics that hitherto were unanticipated, namely the importance of the recirculating region driving a return flow that builds up sediments close to the source and the importance of spatially varying turbulent mixing between the plume and underlying return flow that leads to a decreasing detrainment speed with distance from the source.

There are several reasons why the actual conditions for particle transport by glacial meltwater plumes could not be reproduced by the laboratory experiments. Glacier meltwater plumes transport a range of particle sizes from micrometer-sized clay and silt, to sands, and even larger stones. Observations are limited, but coarse sediments are thought to deposit rapidly from where they emerge from the grounding line whereas finer sands and clay are expected to be transported longer distances by the plume from the grounding line. In the experiments it was necessary to work with particles with diameters between 38 and $90\,\mu$m in order to observe settling before the particles were transported to the end of the tank by the plume. Similarly, the finite tank length restricted the Reynolds number of the flow (based on source speed and diameter) to lie between 500 and 1600. Ballotini were used so that the complex process of flocculation by clay in contact with salt water could be neglected [26]. Despite these limitations, the experiments suggest that interactions between plumes emanating from englacial conduits at the grounding line of an ice shelf interact significantly with the ambient fluid creating a return flow and enhanced particle detrainment, both of which influence sedimentation patterns near the grounding line.

For the reasons above, it is overly ambitious to believe the experiments may serve to provide a predictive model for particle settling below an Antarctic ice shelf near the source at its base. Furthermore, there are no direct observations both of the plume near the source and the underlying sediments. Nonetheless, that it may provide a means to test the scalings against future observations, we make a crude prediction for sediment deposition. We assume that for small particles raining out of a turbulent plume with a recirculation region at the source, the depth and length of sediment deposition beyond the recirculation region are reasonably well characterized by $\bar{h}$ and $\bar{\ell}$, respectively given by (3) and (4). Based upon indirect observations and modelling [27, 28], the volume flux associated with different glacial meltwater plumes in West Antarctica is estimated to be on the order of 0.5 cubic kilometers per year. Assuming a glacial meltwater plume emanates from the base of the glacier into the ocean over a length of 10 km, the volume flux per unit width is $Q_0 \simeq 0.002\,\mathrm{m}^2/\mathrm{s}$. We suppose the volume flux into the plume leaving the recirculation region is of the same order as Q_0, i.e. $Q_{p0} \simeq 0.002\,\mathrm{m}^2/\mathrm{s}$. Thus, for micrometer-sized particles with a settling rate on the order of $U_s \simeq 10^{-6}\,\mathrm{m/s}$, the characteristic length scale for particle deposition is estimated to be $\bar{\ell} \simeq 2 \times 10^3\,\mathrm{m}$. Using a loose packing fraction of $p_f = 0.56$ and assuming a particle concentration by volume of $\phi_{p0} = 0.001$, the rate of increase of the sediment depth is estimated to be $2 \times 10^{-9}\,\mathrm{m/s}$, or about 6 cm per year.

Certainly future studies are needed to improve the understanding of sediment deposition from a glacial meltwater plume as it is affected by the recirculation region and turbulence between the plume and the underlying return flow. Although numerical simulations are now beginning to resolve the detailed processes of particles in fluid flow, this problem involving turbulence, stratification and large spatial scales still lies outside the range of what can reliably be modelled computationally. Thus, it is imperative to perform laboratory experiments at larger spatial and temporal scales in order to gain insight into processes driving sedimentation near the foot of a submarine glacier.

ACKNOWLEDGMENTS

The authors are grateful for the technical assistance provided by A. Jensen, and we wish to thank the two reviewers of the manuscript for their helpful comments. This research was made possible due to the National Science Foundation (Grant OCE-1332750) for their support of the WHOI Geophysical Fluid Dynamics Summer School, where much of the work presented here was undertaken. Additional funds were provided to Sutherland by the Natural Sciences and Engineering Research Council (NSERC) of Canada through its Discovery Grant program.

---

[1] C. Schoof and I. Hewitt, "Ice-sheet dynamics," Annu. Rev. Fluid Mech. **45**, 217–239 (2013).

[2] K. W. Nichols, S. Østerhus, K. Makinson, and T. Gammelsrød, "Ice-ocean processes over the continental shelf of the Southern Weddell Sea, Antarctica: A review," Rev. Geophys. **47**, RG3003 (2009).

[3] A. Jenkins, "Convection driven melting near the grounding lines of ice shelves and tidewater glaciers," J. Phys. Oceanogr. **41**, 2279–2294 (2011).

[4] A. Jenkins, "A one-dimensional model of ice shelf-ocean interaction," J. Geophys. Res. **96**, 20,671–20,677 (1991).

[5] J. Smith, T. J. Andersen, M. Shortt, A. Gaffney, M. Truffer, T. Stanton, R. Bindschadler, P. Dutrieux, A. Jenkins, C.-D. Hillenbrand, W. Ehrmann, H. F. J. Corr, N. Farley, S. Crowhurst, and D. G. Vaughan, "Sub-ice-shelf sediments record history of twentieth-century retreat of Pine Island Glacier," Nature **541**, 77–80 (2017).

[6] E. Meiburg and B. Kneller, "Turbidity currents and their deposits," Annu. Rev. Fluid Mech. **42**, 135–156 (2010).

[7] R. T. Bonnecaze, H. E. Huppert, and J. R. Lister, "Particle-driven gravity currents," J. Fluid Mech. **250**, 339–369 (1993).

[8] R. T. Bonnecaze and J. R. Lister, "Particle-driven gravity currents down planar slopes," J. Fluid Mech. **390**, 75–91 (1999).

[9] K. Snow and B. R. Sutherland, "Particle-laden flow down a slope in uniform stratification," J. Fluid Mech. **755**, 251–273 (2014).

[10] F. de Rooij and S. B. Dalziel, "Time- and space-resolved measurements of deposition under turbidity currents," Spec. Publs. int. Ass. Sediment. **31**, 207–215 (2001).

[11] R. S. J. Sparks, R. T. Bonnecaze, H. E. Huppert, J. R. Lister, M. A. Hallworth, H. Mader, and J. Phillips, "Sediment-laden gravity currents with reversing buoyancy," Earth Planet. Sci. Lett. **114**, 243–257 (1993).

[12] C. Gladstone and D. Pritchard, "Patterns of deposition from experimental turbidity currents with reversing buoyancy," Sedimentology **57**, 53–84 (2010).

[13] B. R. Sutherland, M. K. Gingras, C. Knudson, L. Steverango, and C. Surma, "Particle-bearing currents in uniform density and two-layer fluids," Phys. Rev. Fluids **3**, 023801:1–15 (2018), doi:10.1103/PhysRevFluids.3.023801.

[14] E.A. Cowan and R. D. Powell, "Ice-proximal sediment accumulation rates in a temperate glacial fjord, southeastern Alaska," in *Glacial Marine Sedimentation: Paleoclimatic Significance*, Special Paper, Geological Society of America, Vol. 261, edited by J. B. Anderson and G. M. Ashley (Geological Society of America, Boulder, CO, USA, 1991) pp. 61–73.

[15] R. J. Munro and S. B. Dalziel, "Attenuation technique for measuring sediment displacement levels," Expt. Fluids **39**, 600–611 (2005).

[16] B. R. Sutherland and Y.S. Hong, "Sedimentation from particle-bearing plumes in a stratified ambient," Phys. Rev. Fluids **1**, 074302:1–17 (2016), doi:10.1103/PhysRevFluids.1.074302.

[17] R. Mugford and J. Dowdeswell, "Modeling glacial meltwater plume dynamics and sedimentation in high-latitude fjords," J. Geophys. Res. **116**, F01023 (2011).

[18] D. Martin and R. Nokes, "Crystal settling in a vigorously convecting magma chamber," Nature **332**, 534–536 (1988).

[19] R. S. J. Sparks, S. N. Carey, and H. Sigurdsson, "Sedimentation from gravity currents generated by turbulent plumes," Sedimentology **38**, 839–856 (1991).

[20] P. Burns and E. Meiburg, "Sediment-laden fresh water above salt water: linear stability analysis," J. Fluid Mech. **691**, 279–314 (2011).

[21] P. Burns and E. Meiburg, "Sediment-laden fresh water above salt water: Nonlinear simulations," J. Fluid Mech. **762**, 156–195 (2015).

[22] S. D. Jazi and M. G. Wells, "Enhanced sedimentation beneath particle-laden flows in lakes and the ocean due to double-diffusive convection," Geophys. Res. Lett. **43**, 10,883–10,890 (2016).

[23] J. D. Parsons, J. W. M. Bush, and J. P. M. Syvitski, "Hyperpycnal plume formation from riverine outflows with small sediment concentrations," Sedimentology **48**, 465–478 (2001).

[24] B. R. Sutherland and S. B. Dalziel, "Bedload transport by a vertical jet impinging upon sediments," Phys. Fluids **26**, 035103:1–19 (2014), doi:10.1063/1.4867707.

[25] R. E. Britter and P. F. Linden, "The motion of the front of a gravity current travelling down an incline," J. Fluid Mech. **99**, 531–543 (1980).

[26] B. R. Sutherland, K. J. Barrett, and M. K. Gingras, "Clay settling in fresh and salt water," Env. Fluid Mech. , 1–14 (2014), doi:10.1007/s10652-014-9365-0.

[27] I. Joughin, S. Tulaczyk, D. MacAyeal, and H. Engelhardt, "Melting and freezing beneath the Ross ice streams, Antarctica," J. Glaciol. **50**, 96–108 (2004).

[28] A. M. Le Brocq, A. J. Payne, M. J. Siegert, and R. B. Alley, "A subglacial water-flow model for West Antarctica," J. Glaciol. **55**, 879–888 (2009).